

Amphipathic benzoic acid derivatives: Synthesis and binding in the hydrophobic tunnel of the zinc deacetylase LpxC

Hyunshun Shin,^a Heather A. Gennadios,^b
Douglas A. Whittington^{b,†} and David W. Christianson^{b,*}

^aDepartment of Chemistry, University of San Francisco, 2130 Fulton Street, San Francisco, CA 94117-1080, USA

^bRoy and Diana Vagelos Laboratories, Department of Chemistry, University of Pennsylvania, Philadelphia, PA 19104-6323, USA

Received 29 November 2006; revised 15 January 2007; accepted 26 January 2007

Available online 31 January 2007

Abstract—The first committed step in lipid A biosynthesis is catalyzed by uridine diphosphate-(3-*O*-(*R*-3-hydroxymyristoyl))-*N*-acetylglucosamine deacetylase (LpxC), a zinc-dependent deacetylase, and inhibitors of LpxC may be useful in the development of antibacterial agents targeting a broad spectrum of Gram-negative bacteria. Here, we report the design of amphipathic benzoic acid derivatives that bind in the hydrophobic tunnel in the active site of LpxC. The hydrophobic tunnel accounts for the specificity of LpxC toward substrates and substrate analogues bearing a 3-*O*-myristoyl substituent. Simple benzoic acid derivatives bearing an aliphatic ‘tail’ bind in the hydrophobic tunnel with micromolar affinity despite the lack of a glucosamine ring like that of the substrate. However, although these benzoic acid derivatives each contain a negatively charged carboxylate ‘warhead’ intended to coordinate to the active site zinc ion, the 2.25 Å resolution X-ray crystal structure of LpxC complexed with 3-(heptyloxy)benzoate reveals ‘backward’ binding in the hydrophobic tunnel, such that the benzoate moiety does not coordinate to zinc. Instead, it binds at the outer end of the hydrophobic tunnel. Interestingly, these ligands bind with affinities comparable to those measured for more complicated substrate analogue inhibitors containing glucosamine ring analogues and hydroxamate ‘warheads’ that coordinate to the active site zinc ion. We conclude that the intermolecular interactions in the hydrophobic tunnel dominate enzyme affinity in this series of benzoic acid derivatives.

Published by Elsevier Ltd.

1. Introduction

Nearly 600,000 cases of sepsis or septic shock are diagnosed annually in the US, causing an estimated 100,000 deaths per year.^{1,2} Gram-negative bacterial sepsis arises from the systemic response to infection, mainly the overexpression of cytokines and inflammatory mediators in response to macrophage activation by lipopolysaccharide (LPS), which comprises the outer leaflet of the outer membrane of Gram-negative bacteria.^{3–6} The toxic component of LPS is lipid A, which serves as the hydrophobic anchor of LPS and is essential for bacterial survival.^{3–6} As a therapeutic strategy, the inhibition of enzymes in the lipid A biosynthetic pathway will not only kill Gram-negative bacteria, but will also reduce

toxic lipid A concentrations shed by dying bacteria. This therapeutic strategy could allow for improved management of Gram-negative sepsis and has inspired the search for potent inhibitors of UDP-(3-*O*-(*R*-3-hydroxymyristoyl))-*N*-acetylglucosamine deacetylase (LpxC), a zinc enzyme⁷ that catalyzes the first committed step of lipid A biosynthesis.^{8–11} To date, a variety of inhibitors have been developed against LpxC that contain hydroxamate or phosphonate ‘warheads’ for zinc coordination.^{12–20}

The X-ray crystal structure of LpxC from *Aquifex aeolicus* reveals a catalytic zinc ion (Zn^{2+}_A) coordinated by H79, H238, and D242, and a solvent molecule at the base of a ~20 Å-deep active site cleft.²¹ The native enzyme structure was determined in the presence of excess zinc, which resulted in the binding of an inhibitory zinc ion (Zn^{2+}_B) to catalytic residues E78 and H265. Also coordinated to Zn^{2+}_B was a fatty acid interpretable as either myristate or disordered palmitate, and the aliphatic portion of the fatty acid was bound in a hydrophobic tunnel separate from the main active site

Keywords: Lipid A biosynthesis; Zinc enzyme; Hydrophobic tunnel; Enzyme–inhibitor complex.

* Corresponding author. Tel.: +1 215 898 5714; fax: +1 215 573 2201; e-mail: chris@sas.upenn.edu

† Present address: Amgen Cambridge Research Center, One Kendall Square, Building 1000, Cambridge, MA 02139, USA.

cleft (Fig. 1). It was hypothesized that the 3-*O*-(*R*-3-hydroxymyristoyl) group of the substrate occupied this tunnel during catalysis,²¹ and subsequently determined NMR and X-ray crystal structures of *A. aeolicus* LpxC complexed with the substrate analogue inhibitor^{16,19} TU-514 were consistent with this hypothesis.^{22–24}

Importantly, the inhibitory Zn^{2+}_B ion as well as its bound fatty acid are easily dialyzed out of the crystalline LpxC active site, which facilitates the X-ray crystallographic structure determinations of enzyme–inhibitor complexes.^{24,25} However, dialysis of Zn^{2+}_B out of the LpxC active site in the absence of an inhibitor causes the fatty acid to shift such that it coordinates to Zn^{2+}_A with bidentate coordination geometry,²⁵ thereby completing a square pyramidal zinc coordination polyhedron.²⁴ Since lauric acid (dodecanoic acid) binds to LpxC with $K_d = 1 \mu M$,²¹ we hypothesized that an amphipathic carboxylate derivative could serve as a lead for the design of inhibitors. Moreover, since simple fatty acids bind with affinities comparable to those reported for substrate analogues of more complicated design and synthesis (e.g., the substrate analogue inhibitor TU-514 binds with $IC_{50} = 7.0 \mu M$ and $K_i = 0.65 \mu M$),^{16,19} these results strongly suggest that the primary determinants of LpxC-inhibitor affinity are a suitable ‘warhead’ that completes a square pyramidal zinc coordination polyhedron and a pendant ‘tail’ that binds in the hydrophobic tunnel. That the *N*-aroyl-L-threonine hydroxamate CHIR-090 lacks a hexose ring, yet is a slow, tight-binding inhibitor with $K_i \sim 1 nM$,²⁰ is consistent with this view of structure–affinity relationships in the LpxC active site.

Here, we report the synthesis and evaluation of simple amphipathic benzoic acid derivatives designed to bind

in the hydrophobic tunnel of LpxC. Surprisingly, the X-ray crystal structure of LpxC complexed with one of these derivatives reveals a ‘backward’ binding mode in the hydrophobic tunnel. Therefore, intermolecular interactions in the hydrophobic tunnel, and not carboxylate–zinc coordination interactions, appear to be the primary affinity determinants for this series of benzoic acid derivatives.

2. Results and discussion

2.1. Chemistry

Compounds **1–6** and **8** were obtained from commercial sources. The 4-(heptyloxy)-benzoic acid derivatives (compounds **10–13**) were prepared with moderate to good yields (60–80%, unoptimized) from commercially available methyl 4-(hydroxy)benzoates **10a–13a** by treatment with potassium carbonate in acetone, followed by hydrolysis with lithium hydroxide in tetrahydrofuran (THF) (Scheme 1). Compounds **9** and **14** were prepared in similar manner starting with commercially available methyl 2-(4-(hydroxy)phenyl)acetate or methyl 3-(hydroxy)benzoate, respectively. Compound **7** was prepared by the Wittig reaction of heptyltriphenylphosphonium bromide and methyl 4-(formyl)benzoate followed by hydrolysis with lithium hydroxide in THF.

2.2. Binding affinities of amphipathic benzoic acid derivatives

Amphipathic benzoic acid derivatives bind to LpxC from *A. aeolicus* with the affinities reported in Table 1 as determined by isothermal titration calorimetry.

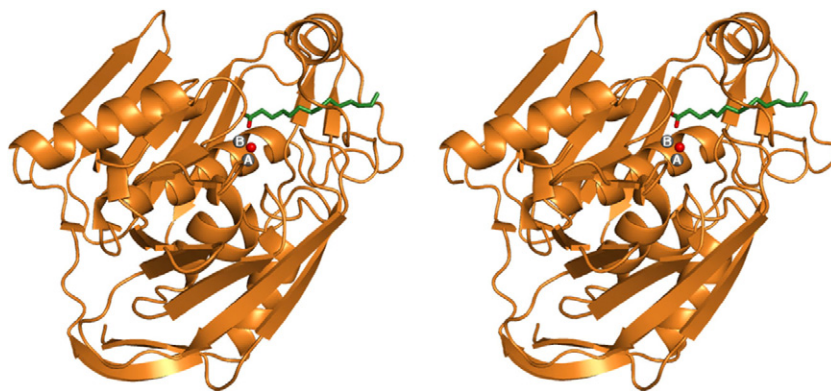
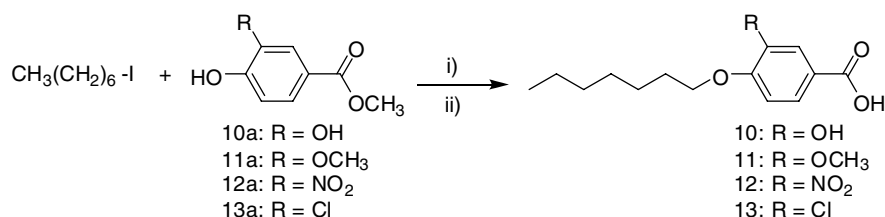
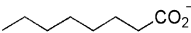
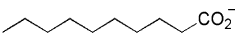
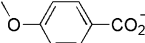
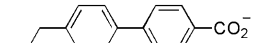
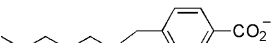
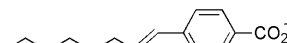
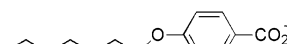
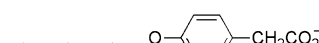
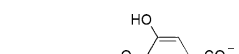
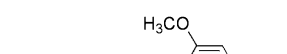
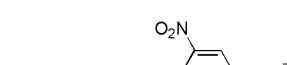
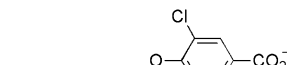
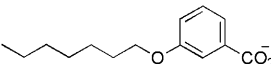


Figure 1. Active site cleft of LpxC; for clarity, only Zn^{2+}_A and Zn^{2+}_B are shown, and the metal-bridging solvent molecule appears as a small red sphere. Myristic acid (green) occupies the hydrophobic tunnel adjacent to Zn^{2+}_B .



Scheme 1. Synthesis of 4-(heptyloxy)benzoic acid derivatives. Reagents: (i) K_2CO_3 /acetone; (ii) LiOH/THF.

Table 1. Amphipathic benzoic acid derivatives and affinities for LpxC

Compound	K_d (μM)
1 	>100 ^a
2 	7.0 ^a
3 	0.9 ^a
4 	No binding
5 	No binding
6 	35
7 	6.2
8 	2.3
9 	2.6
10 	9.0
11 	8.6
12 	6.4
13 	30
14 	2.0

^a Ref. 21.

Micromolar affinity is consistently achieved for compounds bearing a saturated aliphatic ‘tail’ of 10 carbons or longer (compounds **2** and **3**).²¹ Based on the binding of palmitate in the LpxC–palmitate complex,²⁵ the carboxylate group of these ligands had been expected to complete a square pyramidal Zn^{2+} coordination polyhedron in the enzyme active site.

The introduction of rigid C=C double bonds in the ligand skeleton should enhance enzyme–inhibitor affinity by decreasing the entropic cost of freezing out C–C bond rotations required for ligand binding, *if* the

unsaturated ligands can achieve a comparable binding conformation and zinc coordination geometry to that expected for a saturated fatty acid. Benzoic acid derivatives lacking an aliphatic tail do not exhibit measurable binding to LpxC (compounds **4** and **5**). Moreover, the introduction of a *para*-substituted aromatic ring into the pendant tail of a longer fatty acid results in a ~ 35 -fold affinity decrease (compound **6**) compared with compound **3**. At first glance, this might suggest that the introduction of a bulky, conformationally rigid aromatic ring into an aliphatic carboxylate will not enhance enzyme–ligand affinity. However, the introduction of an additional degree of unsaturation into the pendant tail (compound **7**), or the introduction of a polar oxygen atom to generate an aliphatic–aromatic ether (compound **8**), compensates for the observed affinity loss of compound **6**. Lengthening the point of carboxylate attachment to the aromatic ring by a single methylene group has a negligible effect on affinity (compound **9**). The substitution of a single bulky substituent (hydroxy, methoxy, nitro) in the *meta*-position relative to the carboxylate moiety causes only modest (3- to 4-fold) decreases in affinity of the aliphatic–aromatic ether derivative (compounds **10–12**). However, the substitution of a *meta*-chloro substituent decreases affinity 14-fold (compound **13**; since the methoxy and nitro substituents are larger than the chloro substituent, this notable affinity loss is probably not due to a steric effect). A *meta*-substituted aliphatic–aromatic ether (compound **14**) exhibits comparable potency to that of the *para*-substituted isomer (compound **8**). Taken together, these results suggest that substituents at the *para*- and *meta*-positions of the aromatic ring might yield a ‘two-pronged’ inhibitor that could achieve additional binding interactions, for example, as recently demonstrated for certain inhibitors of the zinc enzyme carbonic anhydrase.^{26,27}

2.3. Crystal structure of the LpxC–3-(heptyloxy)benzoate (**14**) complex

The X-ray crystal structure of LpxC complexed with 3-(heptyloxy)benzoate (**14**) (Table 1) determined at 2.25 Å resolution reveals 1:1 enzyme–ligand stoichiometry. An electron density map of the enzyme–ligand complex is found in Figure 2. Ligand binding does not perturb the overall structure of LpxC, and the rms deviations of 267 C α atoms between the zinc-inhibited structure²¹ and the complex with **14** are 0.215 Å. As initially designed, the aliphatic ‘tail’ of **14** is inserted into the active site hydrophobic tunnel. Surprisingly, however, the ligand binds in a ‘backward’ fashion, such that the benzoate carboxylate moiety does not coordinate to Zn^{2+} . Instead, the carboxylate group binds at the outer end of the hydrophobic tunnel and accepts hydrogen bonds from K202 and water molecule #168/#120 (monomer A/B). In monomer A, the carboxylate group also accepts a hydrogen bond from the backbone NH group of L212 from monomer B (Fig. 2).

Curiously, a ‘Y’-shaped peak of electron density corresponds to a nonprotein zinc ligand in the crystal structure of the LpxC complex with 3-(heptyloxy)benzoate, and this electron density cannot be confidently

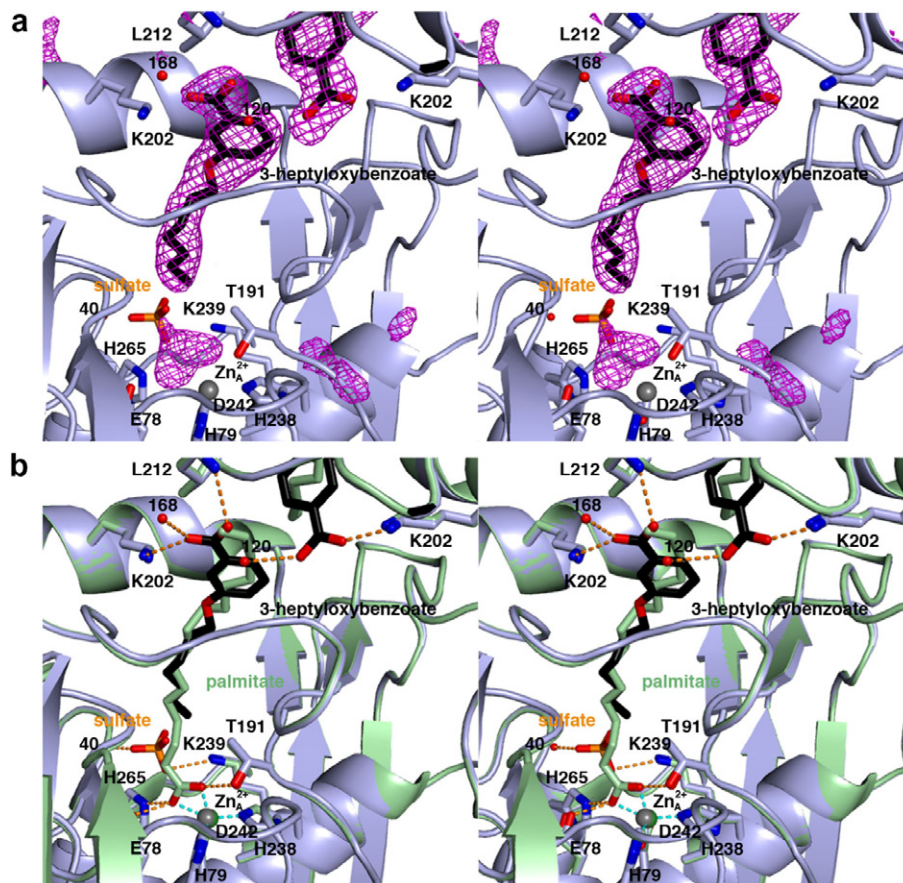


Figure 2. LpxC–3-(heptyloxy)benzoate (**14**) complex (monomer A). (a) Simulated annealing omit electron density map contoured at 4σ (magenta); selected active site residues are indicated. A ‘Y’-shaped electron density peak corresponds to an uninterpretable nonprotein ligand to Zn^{2+} . (b) Hydrogen bond (orange) and metal coordination interactions (cyan) are indicated by dashed lines. Note that 3-(heptyloxy)benzoate binds backward relative to the binding of palmitate,²⁵ which is superimposed in light green. Atoms are color coded as follows: main chain ribbon and side chain carbon atoms, gray (LpxC–3-(heptyloxy)benzoate complex); 3-(heptyloxy)benzoate carbon atoms, black; main chain ribbon side chain carbon and palmitate carbon atoms, green (LpxC–palmitate complex); N, blue; O, red; S, orange; zinc ions appear as gray (LpxC–3-(heptyloxy)benzoate (**14**) complex) or green (LpxC–palmitate complex) spheres; and water molecules appear as small red spheres.

interpreted. This electron density could correspond to an acetate anion; the carboxylate group of an otherwise disordered fatty acid; or, perhaps, a disordered sulfate ion. This electron density is unlikely to correspond to a molecule of 3-(heptyloxy)benzoate bound with its carboxylate coordinated to zinc due to the significant break between the ‘Y’-shaped peak and the peak corresponding to backward-bound 3-(heptyloxy)benzoate (Fig. 2). Nearby, a sulfate ion binds in the ‘basic patch’ of the enzyme active site: in monomer A, sulfate interacts with K239 (3.3 Å) and also hydrogen bonds with water molecule #40; in monomer B, sulfate interacts with K239 (3.5 Å), and the backbone NH groups of H265 and H58.

It should be noted that the ‘Y’-shaped peak of electron density corresponding to the nonprotein zinc ligand was significantly disconnected from the extended electron density in the hydrophobic tunnel even in the initial stages of map calculation and refinement. Although we considered that this peak might correspond to an undisplaced palmitate molecule with its carboxylate group bound to zinc as previously described,²⁵ the interpretation and refinement of palmitate in this structure did not improve

the quality of the electron density in omit maps: disconnected electron density persisted in refinement due to a substantial negative electron density peak between the palmitate C2 and C4 atoms (data not shown). Thus, given that the simulated annealing omit map of 3-(heptyloxy)benzoate in Figure 2 clearly indicates the position of the benzoic acid moiety, and given that the calculation of a simulated omit map minimizes the effects of model bias, we are confident in the interpretation of ligand binding in the LpxC active site as being comprised of one molecule of 3-(heptyloxy)benzoate bound backward in the hydrophobic tunnel, and a separate and possibly disordered carboxylate-containing molecule bound to Zn^{2+} .

There is precedent for the backward binding of amphipathic carboxylates in the hydrophobic tunnel of crystalline LpxC: in the complex with imidazole, the carboxylate group of a fatty acid bound with backward orientation makes no interactions with solvent or with the adjacent monomer in the asymmetric unit;²⁴ in the complex with UDP, the carboxylate group of a fatty acid bound with backward orientation hydrogen bonds with solvent.²⁸ Interestingly, in the complex with 3-(hep-

tyloxy)benzoate, a salt link between the carboxylate and K2O2 may stabilize the backward orientation of the ligand (Fig. 2b). No binding is measurable for 4-heptylaniline (data not shown), which is incapable of making a salt link with K2O2 in a backward orientation or coordinating to zinc in a forward orientation. Therefore, we conclude that a negatively charged carboxylate group is important for binding regardless of the ligand orientation in the hydrophobic tunnel.

While it could be argued that the backward orientation of 3-(heptyloxy)benzoate is an artifact of packing interactions in the crystal lattice, the minimal number of carboxylate interactions observed for ligands bound with backward orientation might suggest that crystal lattice interactions do not play a critical role in governing ligand orientation in the hydrophobic tunnel. If this is the case, then a carboxylate-Zn²⁺_A interaction is not a critical driving force for ligand association. Instead, it follows that binding in the hydrophobic tunnel is the primary affinity determinant for the series of amphipathic benzoic acid derivatives shown in Table 1. Given that a substrate analogue inhibitor bearing the longer 3-*O*-myristic acid substituent is more potent (IC₅₀ = 7.0 μM) than an inhibitor bearing the shorter 3-*O*-hexanoic acid substituent or no substituent at all (IC₅₀ > 3100 μM),¹⁶ van der Waals interactions between the long-chain aliphatic group of an inhibitor and the hydrophobic tunnel appear to make a critical contribution to inhibitor binding that surpasses that of zinc coordination in certain cases.

In conclusion, amphipathic benzoic acid derivatives do not contain an optimal 'warhead' for zinc coordination in the active site of LpxC, based on the observed binding mode of 3-(heptyloxy)benzoate. However, the results reported herein illustrate the importance of interactions in the hydrophobic tunnel and the substantial degree to which the hydrophobic effect drives these interactions to achieve impressive affinity for the binding of relatively simple ligands.

3. Materials and methods

3.1. General synthetic procedures

Unless otherwise specified, materials were purchased from commercial suppliers and used without further purification. Flash chromatography was carried out on Kieselgel 60 (230–400 mesh) and Biotage (Silica Cartridge FLASH 40 + TMS), and analytical thin-layer chromatography was performed on precoated silica gel (60 F254). ¹H and ¹³C spectra were recorded at 500 MHz in CDCl₃, and chemical shifts (δ) are expressed in parts per million relative to residual CHCl₃ at δ = 7.24 ppm for ¹H and to CDCl₃ at δ = 77.0 ppm for ¹³C. ¹H NMR *J* values are reported in Hertz. Mass spectra were recorded at low resolution using Micromass Platform LC spectrometer in electrospray mode and at high resolution with either a VG Micromass 70/70H or VG ZAB-E spectrometer at the University of Pennsylvania.

3.1.1. *n*-Heptylation of methyl hydroxybenzoate derivatives. A solution of 3-substituted-methyl 4-(hydroxy)benzoate (3-substituent = –OH, –OCH₃, –NO₂, or –Cl) or methyl-3-(hydroxy)benzoate, or methyl 2-(4-(hydroxy)phenyl)acetate (5.46 mmol) and anhydrous potassium carbonate (10.7 mmol) in *n*-heptyl iodide (10.7 mmol) and acetone (25 mL) was refluxed for 4–16 h. Evaporation of the solvent and flash chromatography of the residue over silica gel, using 2:8 EtOAc/hexane, gave each desired product as a colorless oil.

3.1.2. Hydrolysis of methyl heptyloxybenzoate derivatives. Aqueous LiOH (2 M, 2 mL) was added to a stirred solution of 3-substituted-methyl 4-(heptyloxy)benzoate or methyl 3-(heptyloxy)benzoate or methyl 2-(4-(heptyloxy)phenyl)acetate (1.13 mmol) in THF (2 mL). Stirring was continued for 2–6 h at 70 °C, and the mixture was acidified with concentrated hydrochloric acid. The mixture was extracted with EtOAc. The combined organic extracts were dried (MgSO₄) and evaporated. Flash chromatography of the residue over silica gel, using 2:8 EtOAc/hexane, gave each of compounds 9–14 as a white solid. Characterization data for each compound are recorded in Sections 3.1.4–3.1.9.

3.1.3. 4-(Oct-1-enyl)benzoic acid (7). To a solution of heptyltriphenylphosphonium bromide (18.3 mmol) in anhydrous THF (30 mL), *n*-BuLi (2.5 M in hexanes, 18.3 mmol) was added dropwise via syringe at room temperature. The reaction mixture was stirred for 15 min and then cooled to 0–4 °C. A solution of methyl 4-formylbenzoate (12.2 mmol) in anhydrous THF (15 mL) was then added dropwise, and the reaction mixture was warmed to ambient temperature and stirred for 1.45 h. The reaction was quenched with saturated aqueous ammonium chloride (25 mL) and extracted with ethyl acetate (EtOAc). Combined organic extracts were dried over magnesium sulfate and evaporated. Flash chromatography of the residue over silica gel, using 2:8 EtOAc/hexane, provided methyl 4-(oct-1-enyl)benzoate (2.1 g, 85%) as a light yellow oil. Hydrolysis of methyl 4-(oct-1-enyl)benzoate was achieved by using the general method outlined above in Section 3.1.2. ¹H NMR (CDCl₃, 500 MHz) δ 0.84–0.89 (m, 3H), 1.25–1.36 (m, 6H), 1.36–1.49 (m, 2H), 2.20–2.34 (m, 2H), 5.75–5.80 (m, 1H), 7.33–7.41 (dd, *J* = 8.2, 8.2 Hz, 2H), 8.00–8.05 (dd, *J* = 8.3, 8.2 Hz, 2H), 8.10 (d, *J* = 2.2 Hz, 1H); high resolution mass spectrum (HRMS) *m/z* calcd for C₁₄H₂₀O₂ 232.1538; found: 232.1538.

3.1.4. 2-(4-(Heptyloxy)phenyl)acetic acid (9). ¹H NMR (CDCl₃, 500 MHz) δ 0.85 (t, *J* = 8.4 Hz, 3H), 1.26–1.38 (m, 8H), 1.63–1.68 (m, 2H), 3.03 (s, 2H), 3.87 (t, *J* = 6.3 Hz, 2H), 6.71 (d, *J* = 8.1 Hz, 2H), 7.04 (d, *J* = 8.1 Hz, 2H); MS (ES+) *m/z* calcd for C₁₅H₂₂O₃ 250.1563; found: 250.30.

3.1.5. 4-(Heptyloxy)-3-hydroxybenzoic acid (10). ¹H NMR (CDCl₃, 500 MHz) δ 0.86–0.88 (m, 3H), 1.22–1.46 (m, 8H), 1.80–1.84 (m, 2H), 4.09 (t, *J* = 6.4 Hz, 2H), 5.63 (s, 1H), 6.86 (d, *J* = 8.4, 1H), 7.62–7.65 (m, 2H); HRMS *m/z* calcd for C₁₄H₂₀O₄ 252.1357; found: 252.1260.

3.1.6. 4-(Heptyloxy)-3-methoxybenzoic acid (11). ^1H NMR (CDCl_3 , 500 MHz) δ 0.87 (t, $J = 7.0$ Hz, 3H), 1.29–1.39 (m, 6H), 1.48–1.51 (m, 2H), 1.83–1.89 (m, 2H), 3.90 (s, 3H), 4.09 (t, $J = 6.5$ Hz, 2H), 7.11–7.13 (m, 1H), 6.94 (d, $J = 8.73$, 1H), 7.95–7.97 (dd, 1H), 8.10 (d, $J = 1.0$ Hz, 1H); ^{13}C NMR (CDCl_3 , 500 MHz) δ 14.0, 22.6, 25.9, 29.0, 31.7, 56.1, 69.12, 111.5, 112.8, 121.2, 124.5, 149.0, 153.5, 170.5; HRMS m/z calcd for $\text{C}_{15}\text{H}_{22}\text{O}_4$ 266.1512; found: 266.1518.

3.1.7. 4-(Heptyloxy)-3-nitrobenzoic acid (12). ^1H NMR (CDCl_3 , 500 MHz) δ 0.87 (t, $J = 6.8$ Hz, 3H), 1.28–1.36 (m, 6H), 1.44–1.44 (m, 2H), 1.82–1.86 (m, 2H), 4.17 (t, $J = 6.5$ Hz, 2H), 7.10–7.12 (d, $J = 8.9$, 1H), 8.21–8.23 (dd, 1H), 8.53 (d, $J = 2.2$ Hz, 1H); ^{13}C NMR (CDCl_3 , 500 MHz) δ 14.0, 22.6, 25.7, 28.7, 28.9, 31.7, 70.2, 113.9, 121.1, 127.8, 135.7, 156.4, 169.6; HRMS m/z calcd for $\text{C}_{14}\text{H}_{19}\text{O}_5\text{N}$ 281.1341; found: 281.1334.

3.1.8. 3-Chloro-4-(heptyloxy)benzoic acid (13). ^1H NMR (CDCl_3 , 500 MHz) δ 0.89 (t, $J = 6.9$ Hz, 3H), 1.29–1.39 (m, 6H), 1.48–1.51 (m, 2H), 1.83–1.89 (m, 2H), 4.09 (t, $J = 6.5$ Hz, 2H), 7.11–7.13 (m, 1H), 6.94 (d, $J = 8.73$, 1H), 7.95–7.97 (dd, 1H), 8.10 (d, $J = 1.0$ Hz, 1H); HRMS m/z calcd for $\text{C}_{14}\text{H}_{19}\text{O}_3\text{Cl}$ 270.1101; found: 270.1102.

3.1.9. 3-(Heptyloxy)benzoic acid (14). ^1H NMR (CDCl_3 , 500 MHz) δ 0.88 (t, 3H), 1.28–1.36 (m, 8H), 1.77–1.80 (m, 2H), 3.99 (t, 2H), 7.11–7.13 (m, 1H), 7.34 (t, 1H), 7.58–7.59 (d, 1H), 7.66–7.67 (dd, 1H); ^{13}C NMR (CDCl_3 , 500 MHz) δ 14.1, 22.6, 26.0, 29.0, 29.2, 31.8, 68.3, 115.1, 120.9, 122.4, 129.5, 130.3, 159.5, 170.73; HRMS m/z calcd for $\text{C}_{14}\text{H}_{20}\text{O}_3$ 236.1412; found: 236.1413.

3.2. Ligand affinity measurements

Ligand binding to *A. aeolicus* LpxC was assayed by isothermal titration calorimetry²⁹ performed at 30 °C on an isothermal microcalorimeter from Microcal, Inc. (Northampton, MA). The enzyme was stripped of all metal ions by dialysis against 1.0 mM EDTA in 25 mM Hepes (pH 7.0), 0.1 M NaCl at room temperature for ≥ 4 h. The EDTA was then removed by extensive dialysis against EDTA-free buffer and the enzyme was reconstituted to a 1:1 Zn^{2+} /LpxC ratio by the addition of ZnSO_4 . A colorimetric assay employing 4-(2-pyridylazo)-resorcinol was used to determine Zn^{2+} concentrations and to verify the preparation of apo and 1:1-reconstituted LpxC as described by Jackman and colleagues.⁷ The calorimeter cell contained either ~ 40 or ~ 60 μM enzyme, and the syringe contained 250 or 400 μM of ligand. A series of 30 injections of 8 μL each were performed at 180-s intervals. Titrations of aliphatic compounds into buffer were also performed as control experiments using identical conditions. Data were fit to a single binding site model using Origin (v. 2.9, Microcal, Inc.). In cases where DMSO was necessary as a carrier solvent to facilitate solubilization of the aliphatic compound of interest, equal amounts of DMSO (vol %) were included in the protein solution.

3.3. Crystallography

The C193A/ Δ D284-L294 variant of LpxC from *A. aeolicus* (henceforth ‘LpxC’) was overexpressed in *Escherichia coli* and purified as described^{7,21} and crystallized using previously reported conditions.²¹ To prepare the enzyme–ligand complex, crystals were gradually transferred to a stabilization buffer containing 100 mM Bis-Tris (pH 6.0), 180 mM NaCl, 14–16% PEG 3350, and 0.5 mM ZnSO_4 . This facilitated the removal of the inhibitory zinc ion, $\text{Zn}^{2+}_{\text{B}}$, which is coordinated by the side chains of E78, H265, and a solvent molecule that bridges the catalytic zinc ion ($\text{Zn}^{2+}_{\text{C}}$) in the structure of the zinc-inhibited enzyme.²¹ Crystals were subsequently transferred to a similar stabilization buffer containing 100 mM Hepes (pH 7.0) and 2 mM 3-(heptyloxy)benzoate, and soaked for approximately 16 h. Diffraction data were measured at the National Synchrotron Light Source at Brookhaven National Laboratories (NSLS, beamline X29A, Upton, NY). Crystals of the enzyme–ligand complex were isomorphous with those of the zinc-inhibited enzyme²¹ and belonged to space group $P6_1$ with unit cell parameters $a = b = 101.0$ Å, $c = 122.7$ Å (two monomers in the asymmetric unit). Data were indexed and merged using *HKL2000*.³⁰ The structure of zinc-inhibited LpxC (PDB entry 1P42),²¹ excluding all zinc ions, solvent, and fatty acid molecules, was used as a search probe in molecular replacement calculations using *AMoRe*.³¹ Initial electron density maps showed that the ligand 3-(heptyloxy)benzoate was bound in the hydrophobic tunnel. Iterative cycles of refinement and model building were performed with *CNS*³² and *O*,³³ respectively, to improve the structure as monitored by R_{free} . Atomic coordinates of solvent molecules and 3-(heptyloxy)benzoate were added during the last stages of refinement of the enzyme–ligand complex. Data collection and refinement

Table 2. Data collection and refinement statistics

Complex	LpxC–compound 14
Resolution range (Å)	50.0–2.25
Reflections (measured/unique)	99618/33203
Completeness (%) (overall/outer shell)	98.8/99.8
R_{merge}^a (overall/outer shell)	0.119/0.508
$\langle I/\sigma \rangle$ (overall/outer shell)	10.4/2.5
Protein atoms (no.) ^b	4298
Solvent atoms (no.) ^b	179
Metal ions (no.) ^b	5
Ligand atoms (no.) ^b	34
Reflections used in refinement (work/free)	31553/1650
R/R_{free} (overall) ^c	0.198/0.227
R/R_{free} (outer shell) ^c	0.242/0.301
rms deviations	
Bonds (Å)	0.006
Angles (deg)	1.2
Proper dihedral angles (deg)	23.4
Improper dihedral angles (deg)	0.8

^a $R_{\text{merge}} = \sum |I_j - \langle I_j \rangle| / \sum I_j$, where I_j is the observed intensity for reflection j and $\langle I_j \rangle$ is the average intensity calculated for reflection j from replicate data.

^b Per asymmetric unit.

^c $R = \sum |F_o| - |F_c| / \sum |F_o|$, where R and R_{free} are calculated using the working and test reflection sets, respectively.

statistics are reported in Table 2. Atomic coordinates of the LpxC–3-(heptyloxy)benzoate complex have been deposited in the Protein Data Bank with accession code 2O3Z.

Acknowledgments

We thank the National Synchrotron Light Source (NSLS) for beamline access. We also thank Dr. Ronen Marmorstein for the use of his instrument for isothermal titration calorimetry experiments with compound **14** and 4-heptylaniline. This work was supported by the National Institutes of Health Grant GM49758.

References and notes

1. Parrillo, J. E. *Ann. Intern. Med.* **1990**, *113*, 227–242.
2. Parrillo, J. E. *N. Eng. J. Med.* **1993**, *328*, 1471–1477.
3. Raetz, C. R. H. *J. Bacteriol.* **1993**, *175*, 5745–5753.
4. Rick, P. D.; Raetz, C. R. H. In *Endotoxin in Health and Disease*; Brade, H., Opal, S. M., Vogel, S. N., Morrison, D. C., Eds.; Marcel Dekker, Inc: New York, 1999; pp 283–304.
5. Wyckoff, T. J. O.; Raetz, C. R. H.; Jackman, J. E. *Trends Microbiol.* **1998**, *6*, 154–159.
6. Raetz, C. R. H.; Whitfield, C. *Ann. Rev. Biochem.* **2002**, *71*, 635–700.
7. Jackman, J. E.; Raetz, C. R. H.; Fierke, C. A. *Biochemistry* **1999**, *38*, 1902–1911.
8. Anderson, M. S.; Bulawa, C. E.; Raetz, C. R. H. *J. Biol. Chem.* **1985**, *260*, 15536–15541.
9. Anderson, M. S.; Robertson, A. D.; Macher, I.; Raetz, C. R. H. *Biochemistry* **1988**, *27*, 1908–1917.
10. Anderson, M. S.; Bull, H. G.; Galloway, S. M.; Kelly, T. M.; Mohan, S.; Radika, K.; Raetz, C. R. H. *J. Biol. Chem.* **1993**, *268*, 19858–19865.
11. Young, K.; Silver, L. L.; Bramhill, D.; Cameron, P.; Eveland, S. S.; Raetz, C. R. H.; Hyland, S. A.; Anderson, M. S. *J. Biol. Chem.* **1995**, *270*, 30384–30391.
12. Onishi, H. R.; Pelak, B. A.; Gerckens, L. S.; Silver, L. L.; Kahan, F. M.; Chen, M.-H.; Patchett, A. A.; Galloway, S. M.; Hyland, S. A.; Anderson, M. S.; Raetz, C. R. H. *Science* **1996**, *274*, 980–982.
13. Chen, M.-H.; Steiner, M. G.; de Laszlo, S. E.; Patchett, A. A.; Anderson, M. S.; Hyland, S. A.; Onishi, H. R.; Silver, L. L.; Raetz, C. R. H. *Bioorg. Med. Chem. Lett.* **1999**, *9*, 313–318.
14. Kline, T.; Andersen, N. H.; Harwood, E. A.; Bowman, J.; Malanda, A.; Endsley, S.; Erwin, A. L.; Doyle, M.; Fong, S.; Harris, A. L.; Mendelsohn, B.; Mdluli, K.; Raetz, C. R. H.; Stover, C. K.; Witte, P. R.; Yabannavar, A.; Zhu, S. *J. Med. Chem.* **2002**, *45*, 3112–3129.
15. Clements, J. M.; Coignard, F.; Johnson, I.; Chandler, S.; Palan, S.; Waller, A.; Wijkman, J.; Hunter, M. G. *Antimicrob. Agents Chemother.* **2002**, *46*, 1793–1799.
16. Jackman, J. E.; Fierke, C. A.; Tume, L. N.; Pirrung, M.; Uchiyama, T.; Tahir, S. H.; Hindsgaul, O.; Raetz, C. R. H. *J. Biol. Chem.* **2000**, *275*, 11002–11009.
17. Pirrung, M. C.; Tume, L. N.; Raetz, C. R. H.; Jackman, J. E.; Snehaltha, K.; McClerren, A. L.; Fierke, C. A.; Gantt, S. L.; Rusche, K. M. *J. Med. Chem.* **2002**, *45*, 4359–4370.
18. Pirrung, M. C.; Tume, L. N.; McClerren, A. L.; Raetz, C. R. H. *J. Am. Chem. Soc.* **2003**, *125*, 1575–1586.
19. Li, X.; Uchiyama, T.; Raetz, C. R. H.; Hindsgaul, O. *Org. Lett.* **2003**, *5*, 539–541.
20. McClerren, A. L.; Endsley, S.; Bowman, J. L.; Andersen, N. H.; Guan, Z.; Rudolph, J.; Raetz, C. R. H. *Biochemistry* **2005**, *44*, 16574–16583.
21. Whittington, D. A.; Rusche, K.; Shin, H.; Fierke, C. A.; Christianson, D. W. *Proc. Natl. Acad. Sci. U.S.A.* **2003**, *100*, 8146–8150.
22. Coggins, B. E.; Li, X.; McClerren, A. L.; Hindsgaul, O.; Raetz, C. R. H.; Zhou, P. *Nat. Struct. Biol.* **2003**, *10*, 645–651.
23. Coggins, B. E.; McClerren, A. L.; Jiang, L.; Li, X.; Rudolph, J.; Hindsgaul, O.; Raetz, C. R. H.; Zhou, P. *Biochemistry* **2005**, *44*, 1114–1126.
24. Gennadios, H. A.; Whittington, D. A.; Li, X.; Fierke, C. A.; Christianson, D. W. *Biochemistry* **2006**, *45*, 7940–7948.
25. Hernick, M.; Gennadios, H. A.; Whittington, D. A.; Rusche, K. M.; Christianson, D. W.; Fierke, C. A. *J. Biol. Chem.* **2005**, *280*, 16969–16978.
26. Roy, B. C.; Banerjee, A. L.; Swanson, M.; Xiao, G. J.; Haldar, M. K.; Mallik, S.; Srivastava, D. K. *J. Am. Chem. Soc.* **2004**, *126*, 13206–13207.
27. Jude, K. M.; Banerjee, A. L.; Haldar, M. K.; Manokaran, S.; Roy, B. C.; Mallik, S.; Srivastava, D. K.; Christianson, D. W. *J. Am. Chem. Soc.* **2006**, *128*, 3011–3018.
28. Gennadios, H. A.; Christianson, D. W. *Biochemistry* **2006**, *45*, 15216–15223.
29. Fisher, H. F.; Singh, N. *Methods Enzymol.* **1995**, *259*, 194–221.
30. Otwinowski, Z.; Minor, W. *Methods Enzymol.* **1997**, *276*, 307–326.
31. Navaza, J. *Acta Crystallogr. A* **1994**, *50*, 157–163.
32. Brünger, A. T.; Adams, P. D.; Clore, G. M.; DeLano, W. L.; Gros, P.; Grosse-Kunstleve, R. W.; Jiang, J.-S.; Kuszewski, J.; Nilges, M.; Pannu, N. S.; Read, R. J.; Rice, L. M.; Simonson, T.; Warren, G. L. *Acta Crystallogr. D* **1998**, *54*, 905–921.
33. Jones, T. A.; Zou, J.-Y.; Cowan, S. W.; Kjeldgaard, M. *Acta Crystallogr. A* **1991**, *47*, 110–119.